

accepted by the The Astrophysical Journal (Letters)

## $\text{N}_2\text{H}^+$ and $\text{C}^{18}\text{O}$ Depletion in a Cold Dark Cloud

Edwin A. Bergin

*Harvard-Smithsonian Center for Astrophysics, 60 Garden Street, Cambridge, MA 02138*

`ebergin@cfa.harvard.edu`

João Alves

*European Southern Observatory, Karl-Schwarzschild-Strasse 2, 85748 Garching, Germany*

`jalves@eso.org`

Tracy L. Huard

*Harvard-Smithsonian Center for Astrophysics, 60 Garden Street, Cambridge, MA 02138*

`thuard@cfa.harvard.edu`

Charles J. Lada

*Harvard-Smithsonian Center for Astrophysics, 60 Garden Street, Cambridge, MA 02138*

`clada@cfa.harvard.edu`

### ABSTRACT

We present sensitive, high angular resolution molecular-line observations of  $\text{C}^{18}\text{O}$  and  $\text{N}_2\text{H}^+$  toward the dark globule B68. We directly compare these data with the near-infrared extinction measurements of Alves, Lada, & Lada (2001) to derive the first evidence for the depletion of  $\text{N}_2\text{H}^+$ , and by inference  $\text{N}_2$ , in a pre-stellar dark cloud. We also find widespread  $\text{C}^{18}\text{O}$  depletion throughout the centrally condensed core of the B68 cloud. Specifically, we find the  $\text{N}_2\text{H}^+$  emission to peak in a shell partially surrounding the peak of dust extinction. Moreover, the  $\text{N}_2\text{H}^+$  peaks inside the much larger  $\text{C}^{18}\text{O}$  depletion hole and has a smaller depletion zone, confirming theoretical predictions. These data are analyzed through a direct coupling of time dependent chemical models to a radiation transfer code. This analysis highlights the importance of photodissociation at cloud edges and suggests that the CO abundance declines by two orders of magnitude from edge to center. In contrast  $\text{N}_2\text{H}^+$  declines in abundance, at minimum, by at least a factor of two. Indeed it is entirely possible that both  $\text{N}_2\text{H}^+$  and  $\text{N}_2$  are completely absent from the central regions of the B68 core. The depletion

of  $\text{N}_2\text{H}^+$ , and its parent molecule  $\text{N}_2$ , opens the possibility that the centers of dense cores, prior to the formation of a star, may evade detection by conventional methods of probing cores using molecular emission. Under these conditions  $\text{H}_2\text{D}^+$  may be the sole viable molecular probe of the innermost regions of star forming cores.

*Subject headings:* ISM:dust, extinction — ISM: abundances — ISM: clouds — ISM: individual (B68) — ISM: molecules — stars: formation

## 1. Introduction

Over the past decade there has been converging observational and theoretical evidence of differential molecular gas phase depletions that tracks the dynamical evolution of star forming cores. This chemical sequence begins with the depletion of sulfur-bearing molecules, which have strong bonds to grain surfaces and are predicted to show the largest depletion “holes” in their emission (Bergin & Langer 1997; Charnley 1997, hereafter BL97 and C97); indeed shell-like structures are now commonly observed for such molecules in low mass cores (e.g., Kuiper, Langer, & Velusamy 1996; Ohashi 2000; Tafalla et al. 2002, hereafter Tf02). Later in the process even volatile molecules, such as CO, deplete; as clearly demonstrated by several observational efforts (Alves et al. 1998; Kramer et al. 1999; Caselli et al. 1999; Jessop & Ward-Thompson 2001).

Besides  $\text{H}_2$ , the molecule predicted to be least affected by the condensation process is  $\text{N}_2$ , which is more volatile than CO and is easily removed from grain surfaces by whatever desorption process acts in molecular cores (BL97; C97). The homonuclear molecule  $\text{N}_2$  is not directly observable, but its chemical daughter products,  $\text{NH}_3$  and  $\text{N}_2\text{H}^+$ , are observed to trace dense cloud cores where other species such as CO and CS are depleted (Bergin et al. 2001, Tf02), consistent with theoretical expectations (BL97, C97, Aikawa et al. 2001; Li et al. 2002).

In this letter we present evidence for the depletion of both  $\text{N}_2\text{H}^+$  and  $\text{C}^{18}\text{O}$  in the cold pre-stellar B68 dark cloud. The detection of  $\text{N}_2\text{H}^+$  depletion opens the possibility that the cores of molecular clouds may evade detection by conventional techniques which rely upon molecules as probes. We discuss the implications of this result for future chemical and star formation studies.

## 2. Telescope and Spectrometers

The  $\text{J}=1-0$  transitions of  $\text{C}^{18}\text{O}$  (109.78218 GHz),  $\text{C}^{17}\text{O}$  (112.359277 GHz), and  $\text{N}_2\text{H}^+$  (93.17378 GHz) were observed during April 2000 and 2001 using the IRAM 30m telescope.  $\text{C}^{18}\text{O}$  was mapped with Nyquist sampling, whereas pointed observations of  $\text{C}^{17}\text{O}$  were conducted using the  $\text{C}^{18}\text{O}$  map as a guide. For  $\text{N}_2\text{H}^+$  the inner  $50''$  of B68 was mapped with Nyquist sampling, but the remainder of the map was obtained with honeycomb ( $24''$ ) spacing. The half-power beam width at 110 GHz and 93 GHz is  $22''$  and  $26''$ , respectively. The system temperatures were typically  $\sim 160$ – $190$  K. In April

2001 we also obtained observations of the J=3-2 transition of  $\text{N}_2\text{H}^+$  (279.512 GHz;  $\theta_{MB} \sim 10''$ ). Each line was observed in frequency switching mode with autocorrelators as the backends providing a velocity resolution of  $0.053 \text{ km s}^{-1}$  ( $\text{C}^{18}\text{O}$ ),  $0.02 \text{ km s}^{-1}$  ( $\text{N}_2\text{H}^+$  3-2), and  $\sim 0.1 \text{ km s}^{-1}$  ( $\text{N}_2\text{H}^+$  1-0,  $\text{C}^{17}\text{O}$ ). Pointing was checked frequently on nearby point sources (in April 2001 Mars was located only  $9^\circ$  from B68) yielding an uncertainty of  $\sim 3''$ . The data were calibrated using the standard chopper wheel method and are presented here on the  $T_{mb}$  scale using standard calibrations from IRAM documentation.

### 3. CO and $\text{N}_2$ Depletion

#### 3.1. Observations

In Figure 1a and 1b we compare the integrated intensity distribution of  $\text{C}^{18}\text{O}$  J=1-0 and  $\text{N}_2\text{H}^+$  J=1-0 (all hyperfine components) with the map of visual extinction ( $A_V$ ) obtained by Alves, Lada, & Lada (2001, hereafter ALL01). The  $\text{C}^{18}\text{O}$  emission peaks in a partial shell-like structure with a radius  $\sim 50''$ , approximately centered on the  $A_V$  peak. Likewise, the  $\text{N}_2\text{H}^+$  emission maxima form an arc centered on the  $A_V$  peak, but lie interior to the  $\text{C}^{18}\text{O}$  shell.

In Figure 2a we present a direct position-by-position comparison to the visual extinction data using the techniques first described in Lada et al. (1994). For  $\text{C}^{18}\text{O}$  there is little scatter with the main feature being a dramatic break in the linear rise in CO emission with visual extinction at  $A_V \sim 8 \text{ mag}$ . This break is followed by a slow but systematic *decrease* in CO emission at greater extinctions. As discussed by Lada et al. (1994), in the absence of non-LTE excitation (as expected for  $\text{C}^{18}\text{O}$ ), a linear correlation between integrated intensity and  $A_V$  corresponds to a constant abundance throughout the cloud. A break in the correlation toward greater extinction could be the result of either a decrease in molecular abundance or high opacity saturating the molecular emission. However, the more optically thin  $\text{C}^{17}\text{O}$  emission ( $\tau \sim 0.4$ ), shown in the lower right of Figure 1b, displays similar behavior and does not increase for  $A_V > 10 \text{ mag}$  and we therefore interpret the structure seen in Figure 1a and 2a as the result of CO depletion. A similar conclusion, using  $^{13}\text{CO}$  and  $\text{C}^{18}\text{O}$  data, has been reached by Hotzel et al. (2002).

In Figure 2b we present the  $\text{N}_2\text{H}^+$  J=1-0 and J=3-2 (2 detections) integrated intensity as a function of  $A_V$ . In Figure 1b the  $\text{N}_2\text{H}^+$  emission exhibits a local minima at the location of the  $A_V$  peak. In Figure 2b this minima is not clearly evident, and the positions in the depression are located as a cluster of points with  $\int T_{mb} dv \sim 2.25 \text{ K km s}^{-1}$  for  $A_V > 25 \text{ mag}$ . A definitive conclusion regarding  $\text{N}_2\text{H}^+$  depletion is complicated by the presence of a few points at similar cloud depths with high intensities (points located as the maxima on the “ring” in Figure 1b). We find no difference between the opacity derived from fits to the hyperfine structure from emission in the “ring” and emission coincident with the depression. However, due to the known presence of excitation gradients in B68 (ALL01) and the expectation of significant non-LTE excitation for  $\text{N}_2\text{H}^+$ , simple conclusions regarding depletion cannot be drawn from Figure 2b (e.g., Bergin et al.

2001).

One additional notable feature in Figure 2b is the lack of significant  $\text{N}_2\text{H}^+$  emission for  $A_V < 5$  mag. A similar threshold is found in IC 5146 by Bergin et al. (2001), which can be interpreted as a decrease in the  $\text{N}_2\text{H}^+$  abundance due to photodestruction of  $\text{N}_2$  by the interstellar radiation field (ISRF).

### 3.2. Chemistry and Radiation Transfer

To determine molecular abundances as a function of cloud depth we have coupled the results from chemical models to a 1-D spherical Monte-Carlo radiation transfer model (Ashby et al. 2000). Our procedure is an iterative one in which we first estimate the radial abundance profile for a given species from a time-dependent chemical model in which we fix profiles of the radial density,  $n_{\text{H}_2}(r)$ , and kinetic temperature,  $T(r)$ . The calculated abundance profile, along with the adopted density and temperature profiles, are then incorporated as input to the radiation transfer model (see Tf02). The radiative transfer model determines the expected profile of integrated intensity, which is convolved to the appropriate angular resolution to compare directly to the observed data<sup>1</sup>. The parameters of the chemical model are then adjusted until the predicted integrated intensity profile matches the observed one. For example, for CO the variables in this iterative solution are: the magnitude of the incident local ISRF, the binding energy of CO to grains (effectively the desorption rate), and time.

We fix the radial density profile used in the chemical and radiative transfer models to that determined from the extinction profile (ALL01). Further, we adopt as the temperature profile that derived for dust in pre-stellar Bonnor-Ebert spheres by Zucconi, Walmsley, & Galli (2001), assuming  $T_{\text{dust}} = T_{\text{gas}}$ . However, we adjust the temperature profile by a uniform reduction of 2 K in order to match the observed intensities of both  $\text{N}_2\text{H}^+$  transitions at the center of the cloud. Although the molecular data in B68 show evidence for systematic velocity gradients (Lada et al. 2002), we assume a static cloud in the radiative transfer model, which may overestimate the line opacities. However, we do incorporate the observed variation in the spectral line width in the model. The model line width includes contributions from the thermal and turbulent widths, with the latter increasing as a function of radius. To be successful a model must reproduce both the dependence of  $\int T dv$  with  $A_V$  (i.e., Figure 2) and  $\Delta v$  with radius (not shown).

---

<sup>1</sup>Similar to Tf02 for  $\text{N}_2\text{H}^+$ , we calculate the level excitation without accounting for hyperfine splitting, but include the effects of the splitting in the calculation of the emergent spectrum (for more discussion see Tf02).

### 3.2.1. $C^{18}O$

For the chemistry of CO we adopted the time dependent analytical expression given by Caselli et al. (2002). This model assumes that there is no gas phase CO formation and destruction, only depletion onto grain surfaces and evaporation by cosmic ray impacts (using the formalism of Hasegawa & Herbst (1993)). In the model, CO starts with an equilibrium abundance of  $x(\text{CO}) = 8.5 \times 10^{-5}$  (relative to  $\text{H}_2$ ) and is allowed to adsorb and desorb. Because we have information on the abundance at cloud edges we also account for  $C^{18}O$  photodestruction using approximations of van Dishoeck & Black (1988). We further adopted the standard ISRF (Habing 1968).

Due to the inclusion of  $C^{18}O$  self-shielding, the model is solved by lagging the solution of the CO column behind the abundance determination. Similar to Caselli et al. (2002) and Aikawa et al. (2001) no solution is found consistent with a CO binding energy,  $E_b = 960$  K. Adopting  $E_b = 1210$  K we find a solution at  $t \sim 6 - 7 \times 10^4$  years<sup>2</sup>. The abundance profile derived from this model is given in Figure 3 and the comparison to the observations is given in Figure 2a. To match the observed structure at low extinction required reducing the UV field by adding an additional 1 mag of extinction to the model. This model provides an excellent fit to the  $C^{18}O$  data from  $A_V = 1$  to 27 mag and suggests that the  $C^{18}O$  abundance declines by over 2 orders of magnitude from  $A_V = 1.5$  to the center.

### 3.2.2. $N_2H^+$

Because of the large number of potential gas phase reaction partners for  $N_2H^+$  we used the chemical model described in BL97. The initial chemical abundances are set to evolved cloud abundances taken from Aikawa et al. (1996), except  $x(\text{CO}) = 8.5 \times 10^{-5}$  and  $x(\text{N}_2) = 2 \times 10^{-5}$ . In addition we use  $E_b(\text{CO}) = 1210$  K and  $E_b(\text{N}_2) = 750$  K. This model is run until the time matched the timescale determined by the CO analysis at which point the theoretical CO abundance profiles predicted by the two models were compared and found to be in good agreement.

In this fashion the abundance of CO, a major destroyer of  $N_2H^+$ , is fixed and the primary variables that alter the  $N_2H^+$  concentration are the abundance of heavy metals and the binding energy of its pre-cursor  $\text{N}_2$ . Changing the metal ion abundances will uniformly change the destruction rate of  $N_2H^+$  at depths  $> 3$  mag (where carbon is not ionized). In contrast, raising  $\text{N}_2$  binding energy will decrease the formation rate in high density regions where depletion dominates.

No match to the data given in Figure 2b is found for a constant  $N_2H^+$  abundance. An abundance reduction at cloud edges is required and the predicted emission does not fit the cluster of data points corresponding to the emission depression discussed in §3.1. If we fix the metal ion

---

<sup>2</sup>As discussed in BL97 (and references therein) a CO binding energy of 960 K is for CO bound to a CO ice covered surface, and 1210 K is representative of CO frozen on a bare silicate surface.

abundances to the values given by Williams et al. (1998), we can match both the  $J = 1 - 0$  and  $J = 3 - 2$  emission, provided we lower the Zucconi, Walmsley, & Galli (2001) temperature profile uniformly by 2 K (as mentioned earlier) and raise the  $N_2$  binding energy to  $E_b(N_2) = 900$  K.

The “best” match abundance profiles for B68 are given in Figure 3 and the fit to the observed emission is shown as a solid curve in Figure 2b. The  $N_2H^+$  abundance profile includes a reduction at cloud edges, peaks at  $A_V = 2$  mag with  $x(N_2H^+) = 6 \times 10^{-11}$ , and declines by a factor of two by  $A_V = 17$  mag. Over this range the concentration of  $N_2$  declines by a factor of 5. *The abundance profile, and  $N_2H^+$  depletion, is constrained by the observations and the radiative transfer;* however, the parameters of the chemical model may not be unique. For example, the  $N_2H^+$  abundance is sensitive to  $E_b(N_2)$  and the ionization fraction. Observations of other molecular ions, which we are in the process of obtaining, will better constrain the ionization fraction and the binding energy.

#### 4. Discussion

Our observations and analysis provide compelling evidence for the existence of CO depletion in B68. Perhaps the most interesting result of our experiment, however, is the finding of  $N_2H^+$  depletion. The robustness of this result depends on the validity of our assumptions. The density profile is well constrained by observations, but the temperature structure is not. B68 is a pre-stellar core; hence the most likely dependence is the adopted one with hot edges and a cold center. Moreover, the detection of  $N_2H^+$   $J = 3 - 2$  in the core center constrains the temperature in the region where depletion is dominant. Opacity is a concern. The Monte-Carlo radiation transfer properly handles the photon propagation, but we have not accounted for the hyperfine structure or systematic line center velocity motions. However, these effects would reduce the opacity, and re-enforce the claim of depletion. Consequently the evidence for  $N_2H^+$  depletion in B68 is relatively firm. In our best fit model we have chosen to fit between the scatter of points at  $A_V > 20$  mag and not the points in the emission depression. Thus we likely have underestimated the  $N_2H^+$  and  $N_2$  depletion. Indeed it is entirely possible that  $N_2$  is almost completely frozen out in the dense center of B68, similar to CO.

Depletion has been found to characterize the inner regions of many quiescent cloud cores. The chemical daughter products of  $N_2$  ( $N_2H^+$  and  $NH_3$ ) have previously been identified as the best available tracers of these regions. However, our finding of  $N_2H^+$  depletion opens the possibility that the very centers of dense cores could be effectively opaque to conventional methods of observation. One casualty of this unfortunate situation is the search for infall wings using optically thin molecular emission (Rawlings et al. 1992) will be hampered by depletion in the very regions where the infall speed is highest. However, because  $H_2$  does not deplete onto grains, its chemical daughter product,  $H_2D^+$ , could therefore prove to be the best tracer of gas in the innermost regions of pre-stellar molecular cores. Indeed, because of  $N_2$  and CO depletion, the abundance of  $H_2D^+$  is expected to be large (Brown & Millar 1989).

Of course, B68 could be a unique object and may be more stable than cores like L1544. This would allow for chemistry to evolve over longer times, resulting in greater freeze out. Alternatively, Charnley & Rodgers (2001) showed that selective depletion could lead to  $\text{N}_2$  destruction by gas-phase chemistry, primarily at longer timescales and higher densities. Because of the potential implications of near complete molecular freeze-out, additional searches for  $\text{N}_2\text{H}^+$  and  $\text{NH}_3$  depletion are needed to infer the general applicability of this result. Regardless, our observations and analysis provide important constraints on the chemical evolutionary processes active in the B68 cloud.

We are grateful to the referee, Steve Charnley, for helpful comments. This work was supported by Grant #NAG5-9520 from NASA's Origins Program.

## REFERENCES

- Aikawa, Y., Ohashi, N., Inutsuka, S., Herbst, E., & Takakuwa, S. 2001, *ApJ*, 552, 639
- Aikawa, Y., Miyama, S. M., Nakano, T., & Umebayashi, T. 1996, *ApJ*, 467, 684
- Alves, J., Lada, C. J., & Lada, E. A. 2001, *Nature*, 409, 159 (ALL01)
- Alves, J., Lada, C. J., Lada, E. A., Kenyon, S. J., & Phelps, R. 1998, *ApJ*, 506, 292
- Ashby, M. L. N. et al. 2000, *ApJ*, 539, L115
- Bergin, E. A. & Langer, W. D. 1997, *ApJ*, 486, 316 (BL97)
- Bergin, E. A., Ciardi, D. R., Lada, C. J., Alves, J., & Lada, E. A. 2001, *ApJ*, 557, 209
- Brown, P. D. & Millar, T. J. 1989, *MNRAS*, 237, 661.
- Caselli, P., Walmsley, C. M., Zucconi, A., Tafalla, M., Dore, L., & Myers, P. C. 2002, *ApJ*, 565, 344
- Caselli, P., Walmsley, C. M., Tafalla, M., Dore, L., & Myers, P. C. 1999, *ApJ*, 523, L165
- Charnley, S. B. & Rodgers, S.D. 2001, *ApJ*, 569
- Charnley, S. B. 1997, *MNRAS*, 291, 455 (C97)
- Habing, H. J. 1968, *Bull. Astron. Inst. Netherlands*, 19, 421
- Hasegawa, T. I. & Herbst, E. 1993, *MNRAS*, 261, 83
- Hotzel, S., Harju, J., Juvela, M., Mattila, K., & Haikala, L.K. 2002, *A&A*, submitted
- Jessop, N. E. & Ward-Thompson, D. 2001, *MNRAS*, 323, 1025

- Kramer, C. Alves, J., Lada, C., Lada, E., Sievers, A., Ungerechts, H., & Walmsley, M. 1999, *A&A*, 342, 257
- Kuiper, T. B. H., Langer, W. D. & Velusamy, T. 1996, *ApJ*, 468, 761
- Lada, C. J., Bergin, E.A., Alves, J.A., & Huard, T. 2002, in preparation
- Lada, C. J., Lada, E. A., Clemens, D. P., & Bally, J. 1994, *ApJ*, 429, 694
- Li, Z., Shematovich, V.I., Wiebe, D.S., Shustov, B.M. (2002), *ApJ*, in press
- Ohashi, N. 2000, *Astrochemistry: From Molecular Clouds to Planetary*, I.A.U. 197, 61
- Rawlings, J. M. C., Hartquist, T. W., Menten, K. M., & Williams, D. A. 1992, *MNRAS*, 255, 471
- Tafalla, M., Myers, P.C., Caselli, P., Walmsley, C.M., & Comito, C. 2002, *ApJ*, in press (Taf02)
- van Dishoeck, E. F. & Black, J. H. 1988, *ApJ*, 334, 771
- Williams, J. P., Bergin, E. A., Caselli, P., Myers, P. C., & Plume, R. 1998, *ApJ*, 503, 689
- Zucconi, A., Walmsley, C. M., & Galli, D. 2001, *A&A*, 376, 650



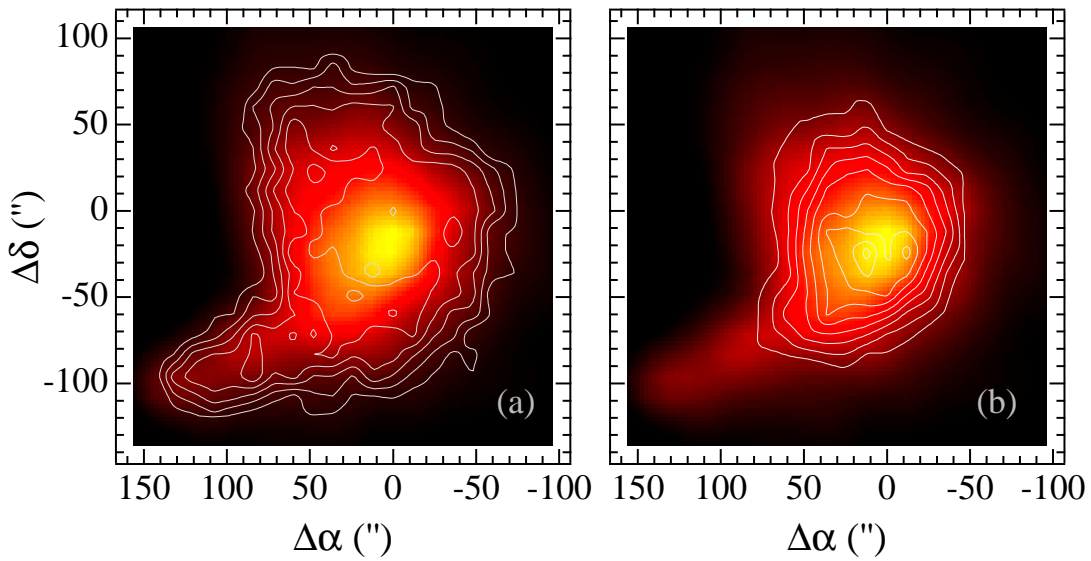


Fig. 1.— (a) Comparison of  $C^{18}O$  J=1-0 integrated emission (contours) in B68 superimposed on a map of visual extinction derived by ALL01 and convolved to the IRAM resolution. The  $C^{18}O$  contours begin at  $0.2 \text{ K km s}^{-1}$  and step in units of  $0.1 \text{ K km s}^{-1}$ . The  $A_V$  image scales is scaled from 0–27 mag. (b) Comparison of  $N_2H^+$  J=1-0 integrated emission (contours) and the visual extinction image. The  $N_2H^+$  contours begin at  $0.3 \text{ K km s}^{-1}$  and step in units of  $0.2 \text{ K km s}^{-1}$ . These maps were referenced to  $\alpha = 17^h 22^m 38^s.2$  and  $\delta = -23^\circ 49' 34''.0$  (J2000). The peak  $A_V$  is located  $6''$  east and  $12''$  south of this position.

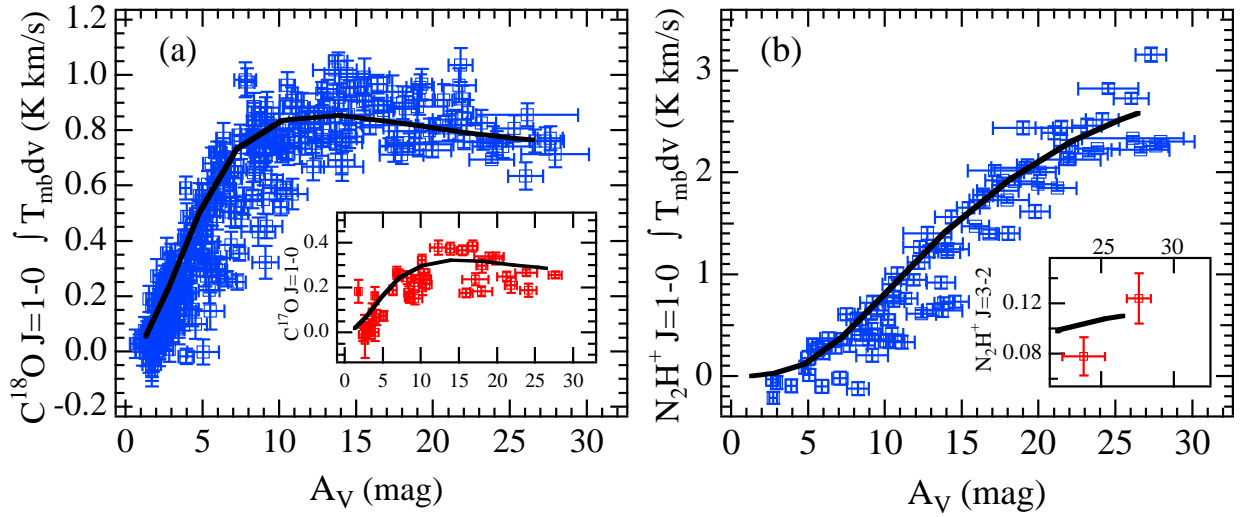


Fig. 2.— (a)  $C^{18}O\ J=1-0$  integrated intensity as a function of visual extinction for the entire B68 dark cloud. Inset to the lower right is a similar plot for  $C^{17}O$ . (b)  $N_2H^+\ J=1-0$  integrated emission as a function of visual extinction in B68. Inset to the lower right are the integrated intensities (in  $K\ km\ s^{-1}$ ) of the 2  $N_2H^+\ J=3-2$  detections at the corresponding extinctions. In all plots the data are presented as open squares with error bars while solid curves represent the emission predicted by a model combining chemistry with a Monte-Carlo radiative transfer code (§3.2). To create these figures the visual extinction data was convolved to a angular resolution of  $25''$  and sampled on the same grid as the molecular observations. For  $N_2H^+\ J=3-2$  the molecular data and model both have an angular resolution of  $10''$ .

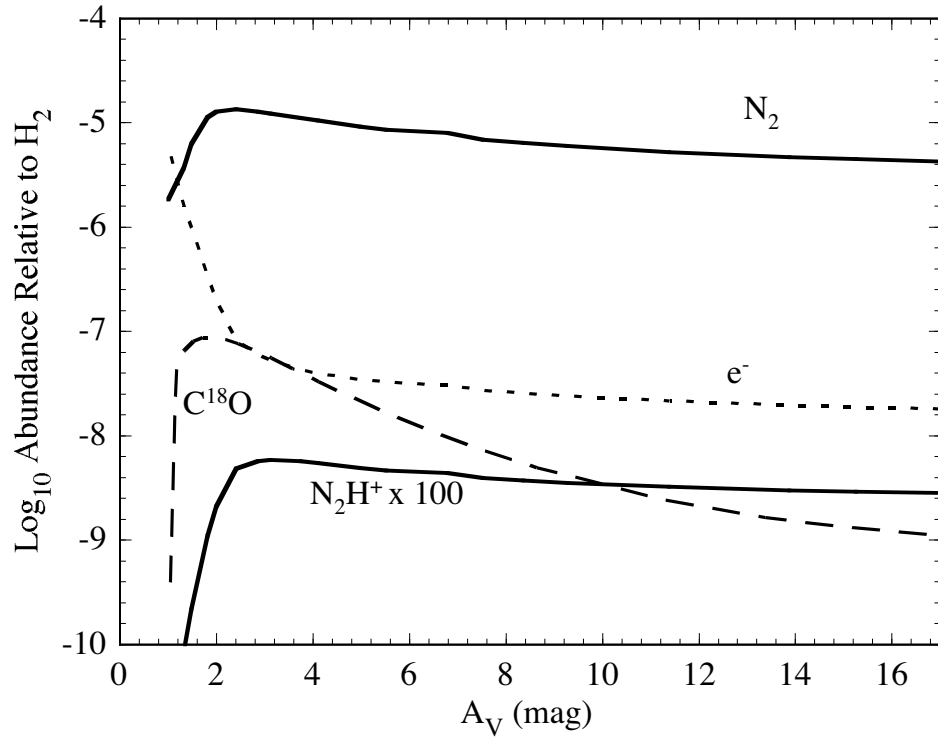


Fig. 3.— Molecular abundances relative to H<sub>2</sub> as a function of visual extinction for the best fit model of B68. The abundance of N<sub>2</sub>H<sup>+</sup> declines by a factor of 2 from A<sub>V</sub> = 2 mag to A<sub>V</sub> = 17 mag.